

**Calibration of the  
Eureka CEC water  
vapour lidar**

A. Moss et al.

**Calibration and validation of water vapour  
lidar measurements from Eureka,  
Nunavut using radiosondes and the  
Atmospheric Chemistry Experiment  
fourier transform spectrometer**

**A. Moss<sup>1</sup>, R. J. Sica<sup>1</sup>, E. McCullough<sup>1</sup>, K. Strawbridge<sup>2</sup>, K. Walker<sup>3</sup>, and  
J. Drummond<sup>4</sup>**

<sup>1</sup>Department of Physics and Astronomy, The University of Western Ontario, London, Canada

<sup>2</sup>Centre for Atmospheric Research Experiments, Environment Canada, Egbert, Canada

<sup>3</sup>Department of Physics, University of Toronto, Toronto, Canada

<sup>4</sup>Department of Physics and Atmospheric Science, Dalhousie University, Halifax, Canada

Received: 7 August 2012 – Accepted: 10 August 2012 – Published: 17 August 2012

Correspondence to: R. J. Sica (sica@uwo.ca)

Published by Copernicus Publications on behalf of the European Geosciences Union.

Title Page

Abstract

Introduction

Conclusions

References

Tables

Figures

◀

▶

◀

▶

Back

Close

Full Screen / Esc

Printer-friendly Version

Interactive Discussion



## Abstract

The Canadian Network for the Detection of Atmospheric Change and Environment Canada DIAL lidar located at the Polar Environment Atmospheric Research Laboratory (PEARL) in Eureka, Nunavut has been upgraded to measure water vapour mixing ratio profiles at 150 m vertical resolution. The system is capable of measuring water vapour in the dry arctic atmosphere up to the tropopause region. Measurements were obtained in the February to March polar sunrise during 2007, 2008 and 2009 as part of the Canadian Arctic ACE Validation Campaign. Before such measurements can be used to address important questions in understanding dynamics and chemistry, the lidar measurements must be calibrated against an independent determination of water vapour. Here, radiosonde measurements of relative humidity have been used to calibrate the lidar measurements. It was found that the calibration varied significantly between each campaign. However, the calibration of the lidar during an individual polar sunrise campaign agrees with the local radiosonde measurements to better than 12 % below 6 km altitude. To independently validate the calibration of the lidar derived from the radiosondes, comparisons are made between the calibrated lidar measurements and water vapour measurements from the Atmospheric Chemistry Experiment satellite-borne Fourier Transform Spectrometer. The comparisons between the lidar and satellite for both campaign averages and single overpasses show favourable agreement between the two instruments and help validate the comparison with the radiosondes.

## 1 Introduction

There are many open questions with regard to water vapour's role in climate and weather. An area of high concern is water vapour's role in Earth's radiative balance, including the various feedbacks involved, both positive (increases in long-wave absorption of solar radiation) and negative (increases in water vapour leading to increases in cloud formation causing cooling due to albedo changes). These feedbacks give rise to

AMTD

5, 5665–5689, 2012

## Calibration of the Eureka CEC water vapour lidar

A. Moss et al.

Title Page

Abstract

Introduction

Conclusions

References

Tables

Figures

◀

▶

◀

▶

Back

Close

Full Screen / Esc

Printer-friendly Version

Interactive Discussion



important yet unresolved questions related to water vapour and its changes in response to a changing climate. Such questions can be addressed with improved measurement capabilities such as those provided by the Canadian Network for the Detection of Atmospheric Change (CANDAC) instrumentation situated at the Polar Environment Atmospheric Research Laboratory (PEARL) in Eureka, Nunavut.

The goal of this study is to determine a calibration for the CANDAC-Environment Canada Stratospheric Differential Absorption Lidar (DIAL; henceforth the CEC Lidar) water vapour mixing ratio measurements by comparison to water vapour measurements made by locally launched radiosondes. Details of the instrument are given in the next section. The retrieval method is then discussed to show how the calibration factors enter the analysis, then the calibration factors are determined and compared to radiosonde measurements. In Sect. 4 comparisons are made to measurements from the Atmospheric Chemistry Experiment Fourier Transform Spectrometer (ACE-FTS). A polar sunrise climatology of the water vapour mixing ratio for 3 seasons of measurements is given in Sect. 5.

## 2 The CEC lidar

The PEARL at Eureka (80.2° N, 86.4° W) consists of three laboratories, two of which are located near the weather station at sea level. The third is the Ridge Laboratory, located 610 m a.s.l. about 18 km from the weather station. The CEC Lidar was installed there in 1992.

Polar sunrise occurs at Eureka in late February. It is an exciting time to take measurements, as sunlight interacts with the atmosphere for the first time after months of darkness. Polar sunrise is a time of rapid variations in atmospheric chemistry and dynamics resulting in rapid ozone variations. Polar sunrise also gives an opportunity to make coincident measurements with instruments aboard the ACE satellite, which has good coverage above Eureka at this time of year for its solar occultation measurements.

### Calibration of the Eureka CEC water vapour lidar

A. Moss et al.

Title Page

Abstract

Introduction

Conclusions

References

Tables

Figures



Back

Close

Full Screen / Esc

Printer-friendly Version

Interactive Discussion





as well as 406 nm (from Raman water vapour scattering). The light passes through narrow band interference filters before being focussed onto one of five photomultiplier tubes. For the elastic channels a mechanical chopper and neutral density filters are used to attempt to keep the counting electronics linear over the required count-rate range.

The photomultiplier tubes are used in photon counting mode so they are capable of detecting the weak signals from the upper atmosphere as well as the faint Raman signals from water vapour. Photon counting is triggered by an optical pickoff linked to the timing unit which gives a reference for each outgoing laser pulse. In the counting unit, pulses accumulate in bins of fixed duration (and therefore fixed altitude range from the lidar), allowing for a vertical backscatter intensity profile to be obtained. For water vapour mixing ratio measurements, the best combination of channels resulting in the highest signal-to-noise ratio returns are the 385 nm and 406 nm channels, which will be used in the subsequent analysis.

### 3 Calibration from radiosonde measurements

#### 3.1 The water vapour retrieval

Whiteman et al. (1992) gives the following formula relating the water vapour mixing ratio,  $W(z)$ , to the ratio of the nitrogen ( $S_{N_2}$ ) and water vapour photocounts ( $S_{H_2O}$ ):

$$W(z) = C_w \Delta_q^{\text{@}}(z_0, z) \cdot \frac{S_{H_2O}}{S_{N_2}} \quad (1)$$

where the calibration constant,  $C_w$  is

$$C_w = \frac{k_{N_2}}{k_{H_2O}} \cdot \frac{\sigma_{N_2}}{\sigma_{H_2O}} \cdot \frac{M_{H_2O}}{M_{\text{dry}}} \cdot \frac{n_{N_2}}{n_{\text{dry}}} \quad (2)$$

and the ratio of atmospheric transmissions is

## Calibration of the Eureka CEC water vapour lidar

A. Moss et al.

Title Page

Abstract

Introduction

Conclusions

References

Tables

Figures

◀

▶

◀

▶

Back

Close

Full Screen / Esc

Printer-friendly Version

Interactive Discussion



## Calibration of the Eureka CEC water vapour lidar

A. Moss et al.

Title Page

Abstract

Introduction

Conclusions

References

Tables

Figures

◀

▶

◀

▶

Back

Close

Full Screen / Esc

Printer-friendly Version

Interactive Discussion



$$\Delta_{\tau}^W(z_0, z) = \frac{\tau(\lambda_N, z_0, z)}{\tau(\lambda_H, z_0, z)}. \quad (3)$$

The ratio of the transmissions is both height and wavelength dependent. In order to estimate the transmission at the two Raman wavelengths, the MODTRAN model (Berk et al., 1998) is used assuming clear sky conditions. This ratio is only weakly height dependent, particularly over the region of CEC Lidar water vapour measurements.

The calibration constant depends on several factors, including the ratio of the detector quantum efficiencies ( $k$ ), the ratio of the Raman cross sections ( $\sigma$ ) and the ratio of the molecular mass ( $M$ ) of water vapour to nitrogen. The final term is the proportion of nitrogen in dry air ( $n_{N_2}/n_{\text{dry}}$ ), allowing  $W(z)$  to be expressed as a mixing ratio by assuming the ratio of nitrogen to oxygen in dry air is constant. The calibration constant is, however, not strictly constant with height, though it will be treated as such hereafter. The cross section term has a weak temperature dependence, that, depending on the bandwidth and blocking of the water vapour interference filter, can vary sufficiently with height and affect the retrieval (Whiteman, 2003). This height variation can be corrected for by modelling combined with knowledge of the nightly temperature profile (say from a radiosonde) or by an empirical correction. For the CEC Lidar measurements the latter option is necessary.

After the atmospheric transmission correction term is applied to the measurements, the calibration constant,  $C_w$ , can be determined. An approximation of this calibration constant is applied to the measurements by including those parameters in the ratio which are known. However, an external source must be used to verify, and possibly correct, this initial value of  $C_w$ .

### 3.2 Calibration

Calibration of lidar water vapour mixing ratios was performed using 11 nights of measurements obtained during the 2008 Canadian Arctic ACE Validation Campaign using

soundings from daily radiosondes launches at 11:15 and 23:15 UT from the Eureka Weather Station.

### 3.2.1 Pre-calibration considerations

Measurements from the radiosondes launched at Eureka are provided by Environment Canada. Both Vaisala RS92 and RS80 model radiosondes were used during the campaigns. The radiosonde relative humidity measurements are converted to mixing ratios using the radiosonde pressure and temperature measurements and the empirical equation of Murphy and Koop (2005) to find the appropriate value of the saturation vapour pressure over ice.

Lidar measurements are generally taken from approximately 03:00 to 08:00 UT, which bracket the radiosonde flights. On some nights rapid variations in water vapour content occur in the period between the 2 flights, making these nights less desirable for calibration.

Another important consideration for comparison with the sondes is that the lidar takes measurements directly overhead at a fixed location, averaged every 10 min and 150 m in altitude, while the radiosonde takes measurements every few seconds as it drifts with the winds. On a given day the balloon may or may not remain in the same air mass as the lidar measurements. This difference is taken into consideration when deciding which radiosonde profiles should be included in the calibration.

### 3.2.2 Determination of the system correction and calibration constant

The calibration was undertaken using nights when the weather was relatively stable, and the individual radiosondes were consistent between both soundings. The calibration based on measurements from the 2008 Canadian Arctic ACE Validation Campaign uses 8 nights of lidar measurements, with 3 nights not included in the calibration due to large changes in water vapour between the two radiosonde flights.

## Calibration of the Eureka CEC water vapour lidar

A. Moss et al.

Title Page

Abstract

Introduction

Conclusions

References

Tables

Figures

◀

▶

◀

▶

Back

Close

Full Screen / Esc

Printer-friendly Version

Interactive Discussion



## Calibration of the Eureka CEC water vapour lidar

A. Moss et al.

Title Page

Abstract

Introduction

Conclusions

References

Tables

Figures

◀

▶

◀

▶

Back

Close

Full Screen / Esc

Printer-friendly Version

Interactive Discussion



A least-squares procedure is used to find a calibration constant that improves the agreement between the radiosondes and the lidar measurements. The calibration constant is found by minimizing the sum of the square of the difference between the radiosonde and lidar water vapour mixing ratio from the surface to the height where the temperature first reaches  $-50^{\circ}\text{C}$ . At temperatures below this threshold, the humidity sensors aboard some radiosondes are known to exhibit significant hysteresis effects (Wade, 1994). For this calibration, such threshold temperatures typically occurred at altitudes between 5.6 to 8.0 km, where the statistical uncertainty of the lidar measurements starts to become large.

The minimization to find the fitting factor is

$$\min = \sum_{i=1}^n (\text{Sonde}_i - (C_w \cdot \text{Lidar}_i))^2 \quad (4)$$

over the specified height range. The calibration constant is then applied to all nights available. Correcting the measurements with this procedure gives excellent agreement in the 2.0 to 4.0 km region, but not outside this range where height dependent differences between the lidar and the sondes becomes large.

### 3.2.3 Height dependent system corrections

For a properly calibrated lidar, the calibration constant discussed in the last section should be independent of height over the entire range of useful measurements. Our first attempt at finding  $C_w$  showed this is not the case. Additional system corrections are required at the lowest and greatest heights.

The nitrogen channel was thought to be linear when installed. It was found after analysis of these measurements that this was not the case. Figure 1 shows the nonlinearity in the system below 2 km. An exponential fit is used to find a correction between 1.24 to 2.59 km. Following this correction, agreement with the radiosondes is much improved, now showing small differences between the radiosonde and lidar below 4 km (Fig. 2). However, a disagreement between the data sets is evident above this altitude.



## Calibration of the Eureka CEC water vapour lidar

A. Moss et al.

Title Page

Abstract

Introduction

Conclusions

References

Tables

Figures

◀

▶

◀

▶

Back

Close

Full Screen / Esc

Printer-friendly Version

Interactive Discussion



The need for a correction above 4 km is likely due in large part to the assumed transmission ratios not being sufficiently accurate. Few measurements of aerosol loading at high latitude are incorporated into MODTRAN. Also, the effect of temperature on the water vapour Raman cross section may be sufficiently large to further contribute to a height dependent correction. To account for these and possible other variations a correction is determined by fitting an exponential to the ratio of the lidar and radiosonde measurements above 4 km (Fig. 3). The lidar returns now show much better agreement with the radiosondes, with minimal bias (Fig. 4).

The least squares procedure is then performed on the system-corrected measurements to find a final fitting factor, using measurements over the entire altitude range. The result of this procedure gives  $C_w = 8.0527$  (Fig. 4). The average percent difference between lidar and radiosonde measurements is about 5.2 % with small bias. At all altitudes, agreement between the lidar and radiosonde water vapour mixing ratios is better than 20 % in the tropopause region. Agreement is even better in the troposphere, with percent difference less than 12 % below 6 km. The nightly-averaged differences between the radiosonde and lidar for individual nights in 2008 using the systematic corrections and final calibration constant is shown in Fig. 5.

Having performed the calibration for measurements in 2008, it was thought that this calibration might be applicable in 2007 and 2009. To check this assertion the calibration factors are found for 2007 and 2009. The factors are not statistically the same as in 2008. This result is not unexpected due to the potential for system parameters and atmospheric conditions to change from year to year (the instrument is mothballed between the polar sunrise measurement periods). Our analysis showed that both the instrumental corrections and calibration factor changed enough that the calibration procedure needs to be repeated each season.

### 3.3 Annual calibrations

Constant corrections are determined for 2007 and 2009 using the same procedures as for 2008, i.e. a subset of nights chosen each year which showed relatively clear-sky

nights and consistent radiosonde measurements. The system correction and calibration constant for each year is given in Table 1. The system correction and calibration constant are similar in shape with a significant different in magnitude.

#### 4 Comparisons with the ACE-FTS

The ACE satellite has been in orbit since August 2003. ACE is comprised of two principle instruments, the ACE-FTS and Measurements of Aerosol Extinction in the Stratosphere and Troposphere Retrieved by Occultation (MAESTRO) which together measure many molecular species of interest in the atmosphere. Both instruments make measurements using a solar occultation method, whereby a reference measurement is taken looking directly at the Sun, then a measurement is taken looking at the Sun through the atmosphere. Bernath et al. (2005) gives an overview of the ACE-FTS instrument, while Boone et al. (2005) gives a detailed description of the analysis of the ACE-FTS measurements.

The ACE-FTS measurements have a different viewing geometry and height resolution than the lidar measurements. For this comparison the lidar measurements have been co-added in height to more closely match the vertical resolution of ACE-FTS (approximately 3 to 4 km). Due to the lack of exact measurement co-location and coincidence, averages for the 2007 and 2008 seasons are used for the comparison. These averages comprise five nights of ACE-FTS measurements in 2007 and four nights in 2008 (Figs. 6 and 7). The error bars used for the ACE-FTS and lidar profiles are the RMS values associated with the campaign averages (which is much greater than the statistical uncertainties). Though the region of overlap between the measurements is limited, the continuity between the independently calibrated instruments is encouraging.

Figure 8 shows an example of comparisons for a single overpass. There are four possible nights for nightly comparisons between the lidar and ACE-FTS. In almost all cases the lidar mixing ratios are about 20 % higher than those from the ACE-FTS. This

### Calibration of the Eureka CEC water vapour lidar

A. Moss et al.

Title Page

Abstract

Introduction

Conclusions

References

Tables

Figures



Back

Close

Full Screen / Esc

Printer-friendly Version

Interactive Discussion



difference may suggest a height bias in the lidar measurements at the upper altitudes, but further comparisons are required.

## 5 Water vapour climatology

A polar sunrise climatology was formed for the 3 periods available (Fig. 9). The nights used in the averages are shown in Table 2. Below 4 km the largest variability in water vapour mixing ratio was in 2007. The large variability seen in the lower troposphere in 2007 may be due to effects of the polar vortex present in the Arctic atmosphere. In 2007 various vortex scenarios were observed above Eureka, with the lidar measuring both inside and outside the vortex, as well as near the vortex edge. The vortex causes great variability in vertical temperature and ozone profiles in the middle and upper atmosphere and may affect water vapour in the upper troposphere and lower stratosphere. In 2009 there are more measurements available than the other years. The variability is smaller at the lowest heights but larger above 4 km compared to 2007 and 2008.

## 6 Conclusions

A water vapour system correction and calibration constant were determined for the CEC Lidar. For this calibration, a comparison was done to measurements made by radiosonde balloons launched twice daily from the nearby Eureka Weather Station. The calibration involves a system (height-dependent) correction, as well as a constant calibration factor determined by least-squares fitting on nights with consistent radiosonde measurements. The calibration is tested on lidar measurements from 2007 and 2009 for inter-annual consistency. Agreement with the radiosondes is poor in 2007 and 2009 using the 2008 calibration, demonstrating that annual calibration efforts are necessary. Statistical uncertainty limits water vapour mixing ratio profiles to between 6 and 8 km. Nightly contours at 10 min time resolution reach altitudes between 5 and 8 km depending on the night.

### Calibration of the Eureka CEC water vapour lidar

A. Moss et al.

Title Page

Abstract

Introduction

Conclusions

References

Tables

Figures



Back

Close

Full Screen / Esc

Printer-friendly Version

Interactive Discussion



## Calibration of the Eureka CEC water vapour lidar

A. Moss et al.

Title Page

Abstract

Introduction

Conclusions

References

Tables

Figures



Back

Close

Full Screen / Esc

Printer-friendly Version

Interactive Discussion



Limitations of the calibration technique used include the lack of both temporal and spatial coincidence between the lidar and radiosonde measurements, as well as the inability of the radiosondes to make reliable humidity measurements in the upper troposphere. To improve this calibration, use of balloon-borne frost point hygrometers would help with calibration of water vapour mixing ratios in the tropopause region. Furthermore, techniques are being developed to improve long-term calibration of water vapour lidar systems, including a hybrid approach involving both radiosondes and a calibration lamp (Leblanc and McDermid, 2008) as well as a first-principle calibration using lamps which scan the entire system field-of-view, eliminating the need to compare to other independent water vapour measurements (Venable et al., 2011). Such methods will be adopted for future PEARL measurements.

*Acknowledgements.* The Atmospheric Chemistry Experiment (ACE), also known as SCISAT, is a Canadian-led mission mainly supported by the Canadian Space Agency and the Natural Sciences and Engineering Research Council of Canada.

The Canadian Arctic ACE Validation campaign project has been supported by the Canadian Space Agency (CSA), Environment Canada (EC), the Natural Sciences and Engineering Research Council (NSERC) of Canada, the Northern Scientific Training Program and the Centre for Global Change Science at the University of Toronto. Logistical and on-site technical support for the 2006–2009 campaigns was provided by the Canadian Network for the Detection of Atmospheric Change (CANDAC).

CANDAC and PEARL research was supported by the Canadian Foundation for Innovation, the Ontario Innovation Trust, the Ontario Research Fund, the Canadian Foundation for Climate and Atmospheric Sciences (CFCAS), the Natural Sciences and Engineering Council (NSERC), Environment Canada, the Polar Continental Shelf Project (PCSP), the Canadian International Polar Year Program, and the Canadian Space Agency (CSA).

In addition, the authors would like to thank the CANDAC and PEARL staff and the PEARL operators for instrument preparation, maintenance and data collection.

## References

- Berk, A., Bernstein, L., Anderson, G., Acharya, P., Robertson, D., Chetwynd, J., and Adler-Golden, S.: MODTRAN cloud and multiple scattering upgrades with application to AVIRIS, *Remote Sens. Environ.*, 65, 367–375, doi:10.1016/S0034-4257(98)00045-5, 1998. 5670
- 5 Bernath, P., McElroy, C., Abrams, M., Boone, C., Butler, M., Camy-Peyret, C., Carleer, M., Clerbaux, C., Coheur, P., Colin, R., DeCola, P., Bernath, P., McElroy, C., Abrams, M., Boone, C., Butler, M., Camy-Peyret, C., Carleer, M., Clerbaux, C., Coheur, P., Colin, R., DeCola, P., DeMaziere, M., Drummond, J., Dufour, D., Evans, W., Fast, H., Fussen, D., Gilbert, K., Jennings, D., Llewellyn, E., Lowe, R., Mahieu, E., McConnell, J., McHugh, M., McLeod, S.,
- 10 Michaud, R., Midwinter, C., Nassar, R., Nichitiu, F., Nowlan, C., Rinsland, C., Rochon, Y., Rowlands, N., Semeniuk, K., Simon, P., Skelton, R., Sloan, J., Soucy, M., Strong, K., Tremblay, P., Turnbull, D., Walker, K., Walkty, I., Wardle, D., Wehrle, V., Zander, R., and Zou, J.: Atmospheric Chemistry Experiment (ACE): mission overview, *Geophys. Res. Lett.*, 32, L15S01, doi:10.1029/2005GL022386, 2005. 5674
- 15 Boone, C., Nassar, R., Walker, K., Rochon, Y., McLeod, S., Rinsland, C., and Bernath, P.: Retrievals for the atmospheric chemistry experiment Fourier-transform spectrometer, *Appl. Optics*, 44, 7218–7231, 2005. 5674
- Carswell, A., Pal, S., and Steinbrecht, W.: Lidar measurements of the middle atmosphere, *Can. J. Phys.*, 69, 1076–1086, 1991. 5668
- 20 Leblanc, T. and McDermid, I. S.: Accuracy of Raman lidar water vapor calibration and its applicability to long-term measurements, *Appl. Optics*, 47, 5592–5603, 2008. 5676
- Murphy, D. and Koop, T.: Review of the vapour pressures of ice and supercooled water for atmospheric applications, *Q. J. Roy. Meteorol. Soc.*, 131, 1539–1565, 2005. 5671
- Pal, S., Carswell, A., Bird, J., Donovan, D., Duck, T., and Whiteway, J.: Lidar measurements of the stratosphere at the Eureka and Toronto NDSC stations, in: *Proceedings of the Conference on Application of Lidar to Current Atmospheric Topics*, edited by: Pal, S. R., York Univ., Inst. Space Terr. Sci., Toronto, ON, Canada, 28–39, 1996. 5668
- 25 Venable, D. D., Whiteman, D. N., Calhoun, M. N., Dirisu, A. O., Connell, R. M., and Landulfo, E.: Lamp mapping technique for independent determination of the water vapor mixing ratio calibration factor for a Raman lidar system, *Appl. Optics*, 50, 4622–4632, 2011. 5676
- 30 Wade, C.: An evaluation of problems affecting the measurement of low relative-humidity on the united-states radiosonde, *J. Atmos. Ocean. Tech.*, 11, 687–700, 1994. 5672

### Calibration of the Eureka CEC water vapour lidar

A. Moss et al.

Title Page

Abstract

Introduction

Conclusions

References

Tables

Figures



Back

Close

Full Screen / Esc

Printer-friendly Version

Interactive Discussion



Whiteman, D.: Examination of the traditional Raman lidar technique, 1. Evaluating the temperature-dependent lidar equations, *Appl. Optics*, 42, 2571–2592, 2003. 5670  
Whiteman, D., Melfi, S., and Ferrare, R.: Raman lidar system for the measurement of water-vapor and aerosols in the Earths atmosphere, *Appl. Optics*, 31, 3068–3082, 1992. 5669

---

**Calibration of the Eureka CEC water vapour lidar**

A. Moss et al.

---

Title Page

Abstract

Introduction

Conclusions

References

Tables

Figures



Back

Close

Full Screen / Esc

Printer-friendly Version

Interactive Discussion



## Calibration of the Eureka CEC water vapour lidar

A. Moss et al.

**Table 1.** System corrections and calibration constants for the 2007 to 2009 Canadian Arctic ACE validation campaigns.

Year	Altitude (km)	Instrumental Correction	Calibration Constant
2007	0.94 < z < 1.84	$1 + 105.8047 \times \exp(-3.9473z)$	7.3379
	1.99 < z < 5.43		
	5.43 < z		
2008	0.94 < z < 2.59	$0.8859 + 521.0029 \times \exp(-5.0703z)$	8.0527
	2.59 < z < 4.08		
	4.08 < z		
2009	0.94 < z < 1.69	$1.0991 + 6670.3 \times \exp(-8.3874z)$	7.9688
	1.69 < z < 3.93		
	3.93 < z		

Title Page

Abstract

Introduction

Conclusions

References

Tables

Figures

◀

▶

◀

▶

Back

Close

Full Screen / Esc

Printer-friendly Version

Interactive Discussion



**Table 2.** Lidar measurements used in the 2007 to 2009 polar sunrise climatology. An “o” for a given date indicates measurements are included in the climatology. An “x” indicates that measurements exist on the date but were not of sufficient quality (primarily due to deteriorating weather over the night) to use in the climatology.

February	2007	2008	2009
8			o
9			o
10			o
11			o
12			o
13			
14			
15			
16			o
17	o	o	o
18	o	o	o
19			o
20			
21	o		o
22	o		o
23		o	o
24		o	o
25		x	o
26			
27	o		
28		o	
29		o	
March	2007	2008	2009
1	o	o	o
2		o	o
3		o	o
4	o	o	
5			o
6	o		o

**Calibration of the Eureka CEC water vapour lidar**

A. Moss et al.

Title Page

Abstract

Introduction

Conclusions

References

Tables

Figures

◀

▶

◀

▶

Back

Close

Full Screen / Esc

Printer-friendly Version

Interactive Discussion





**Calibration of the  
Eureka CEC water  
vapour lidar**

A. Moss et al.

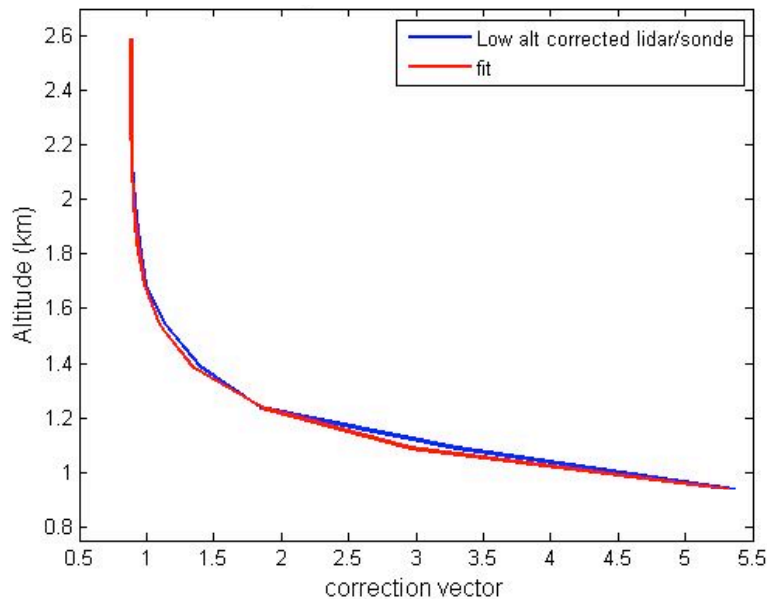


**Fig. 1.** Exponential correction at low altitudes. The red curve is the exponential fit to the calibration data obtained from the comparison of the lidar to the radiosonde measurements (blue curve).

Title Page

Abstract

Introduction

Conclusions

References

Tables

Figures

◀

▶

◀

▶

Back

Close

Full Screen / Esc

Printer-friendly Version

Interactive Discussion



## Calibration of the Eureka CEC water vapour lidar

A. Moss et al.

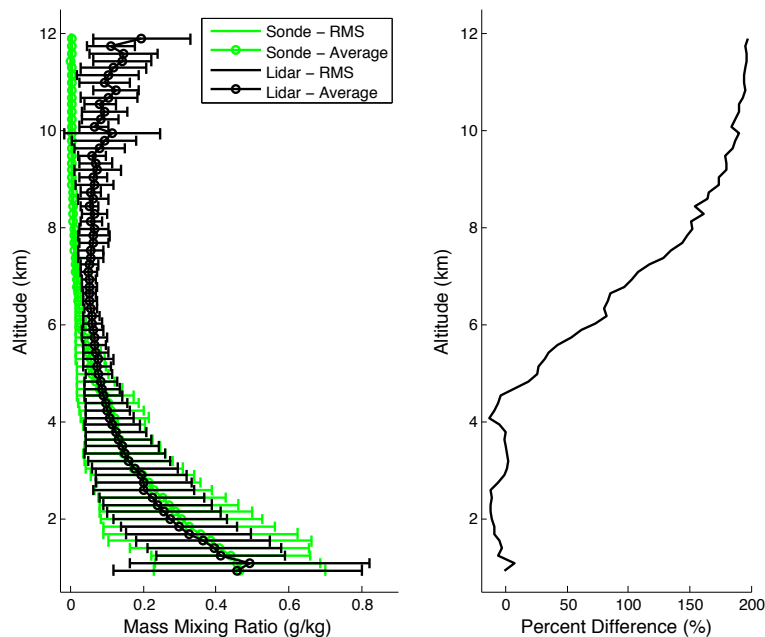


**Fig. 2.** Comparison of the average 2008 lidar and radiosonde measurements. Following the low altitude correction, an additional exponential correction has been applied to the lidar measurements below 2.6 km.

[Title Page](#)[Abstract](#)[Introduction](#)[Conclusions](#)[References](#)[Tables](#)[Figures](#)[◀](#)[▶](#)[◀](#)[▶](#)[Back](#)[Close](#)[Full Screen / Esc](#)[Printer-friendly Version](#)[Interactive Discussion](#)

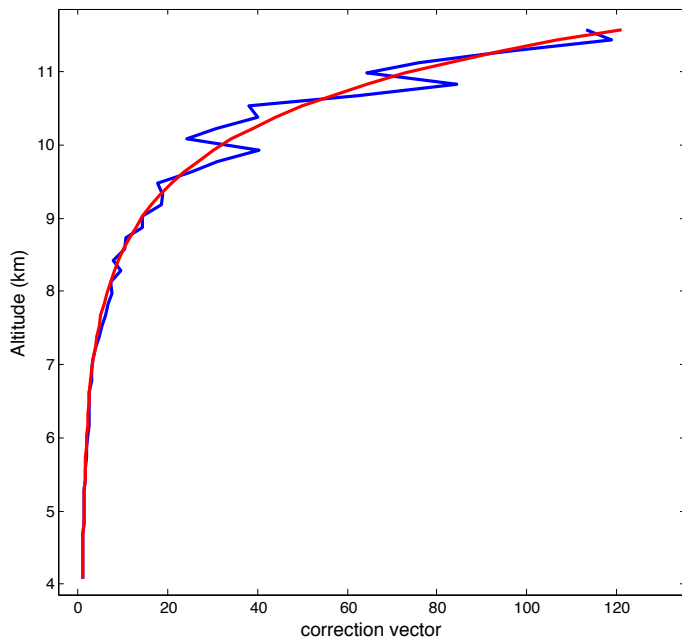


**Fig. 3.** Exponential correction at high altitudes. The red curve is the exponential fit to the calibration data obtained from the comparison of the lidar to the radiosonde measurements (blue curve).

**Calibration of the Eureka CEC water vapour lidar**

A. Moss et al.

Title Page

Abstract

Introduction

Conclusions

References

Tables

Figures

◀

▶

◀

▶

Back

Close

Full Screen / Esc

Printer-friendly Version

Interactive Discussion



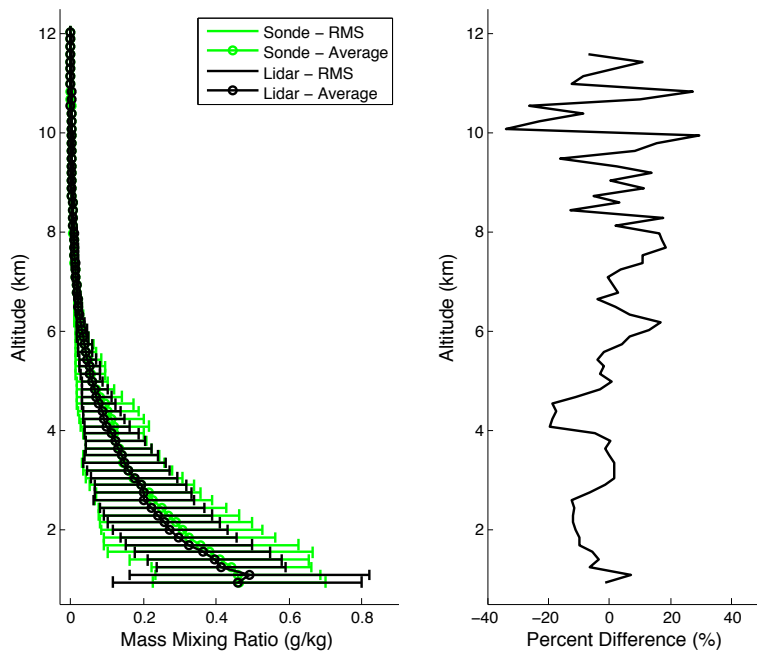


**Fig. 4.** Comparison of the average 2008 lidar and radiosonde measurements. An exponential correction has been applied to the lidar measurements above 4 km. The bias over the entire height range has been reduced to 0.9 %.

**Calibration of the Eureka CEC water vapour lidar**

A. Moss et al.

Title Page

Abstract Introduction

Conclusions References

Tables Figures

◀ ▶

◀ ▶

Back Close

Full Screen / Esc

Printer-friendly Version

Interactive Discussion



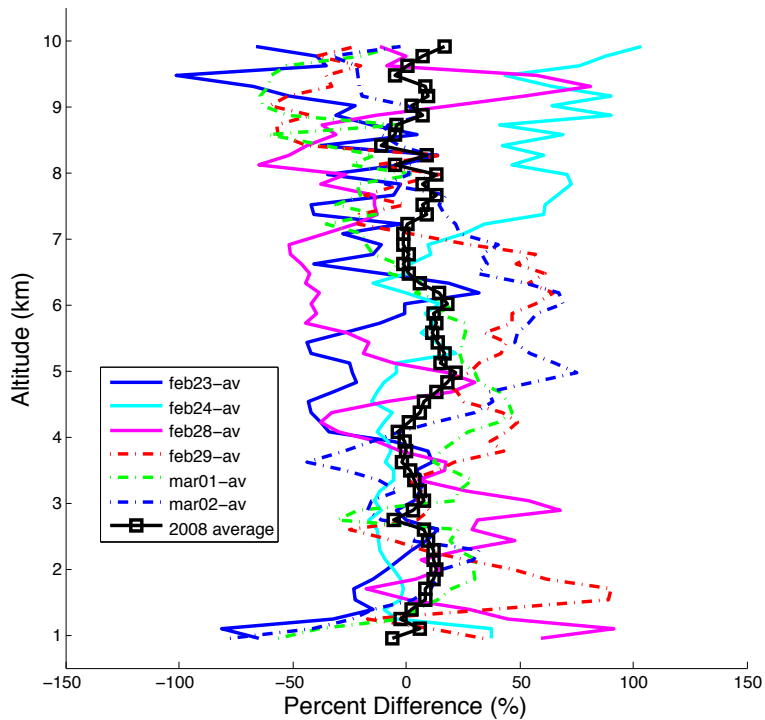


**Fig. 5.** Application of the system and calibration corrections to the 2008 lidar measurements.

**Calibration of the Eureka CEC water vapour lidar**

A. Moss et al.

Title Page

Abstract Introduction

Conclusions References

Tables Figures

◀ ▶

◀ ▶

Back Close

Full Screen / Esc

Printer-friendly Version

Interactive Discussion



## Calibration of the Eureka CEC water vapour lidar

A. Moss et al.

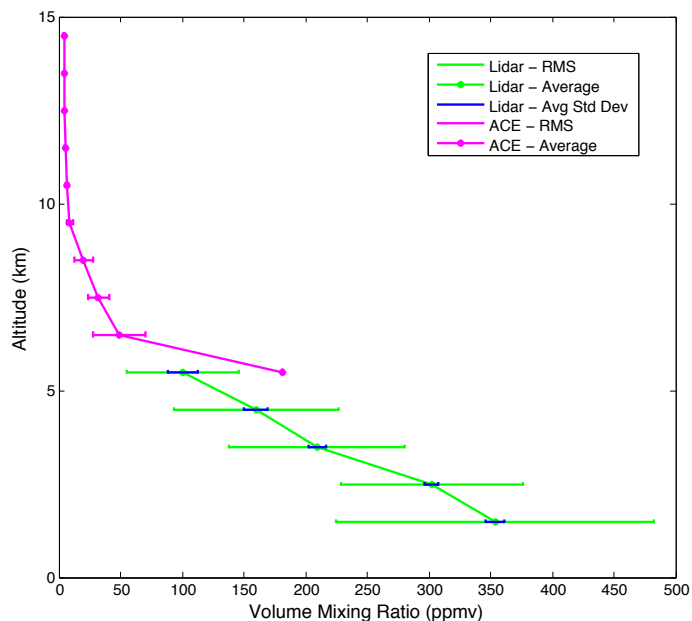


**Fig. 6.** Comparison of water vapour mixing ratio measurements made by the CEC-Lidar and ACE-FTS in 2007. The ACE-FTS profile is the average of all measurements within 200 km (measured from the 30 km point of the ACE-FTS occultation and the CEC-Lidar) made during the Canadian Arctic ACE Validation Campaign period. The lidar profile is the average of the coincident nights. The horizontal bars indicate the RMS deviation of the averages.

[Title Page](#)
[Abstract](#)
[Introduction](#)
[Conclusions](#)
[References](#)
[Tables](#)
[Figures](#)
[◀](#)
[▶](#)
[◀](#)
[▶](#)
[Back](#)
[Close](#)
[Full Screen / Esc](#)
[Printer-friendly Version](#)
[Interactive Discussion](#)


**Calibration of the Eureka CEC water vapour lidar**

A. Moss et al.

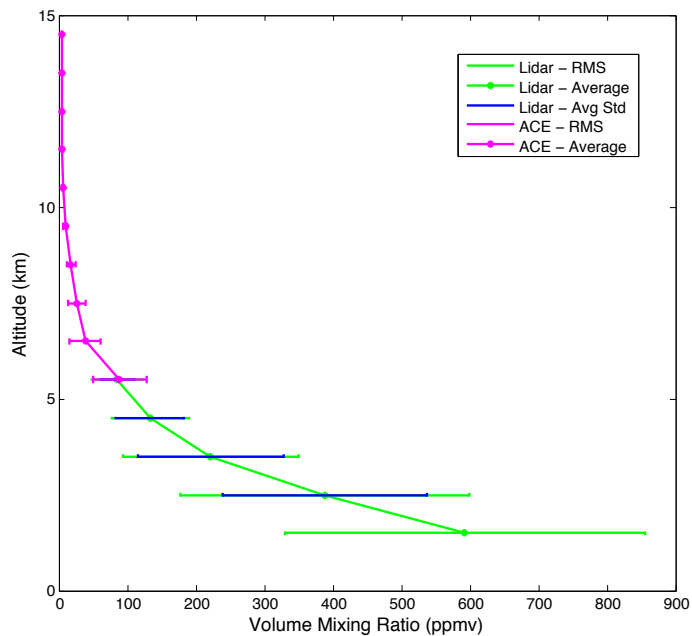


**Fig. 7.** Comparison for the 2008 Canadian Arctic ACE Validation Campaign in the same format as Fig. 6.

Title Page

Abstract

Introduction

Conclusions

References

Tables

Figures

◀

▶

◀

▶

Back

Close

Full Screen / Esc

Printer-friendly Version

Interactive Discussion



**Calibration of the  
Eureka CEC water  
vapour lidar**

A. Moss et al.

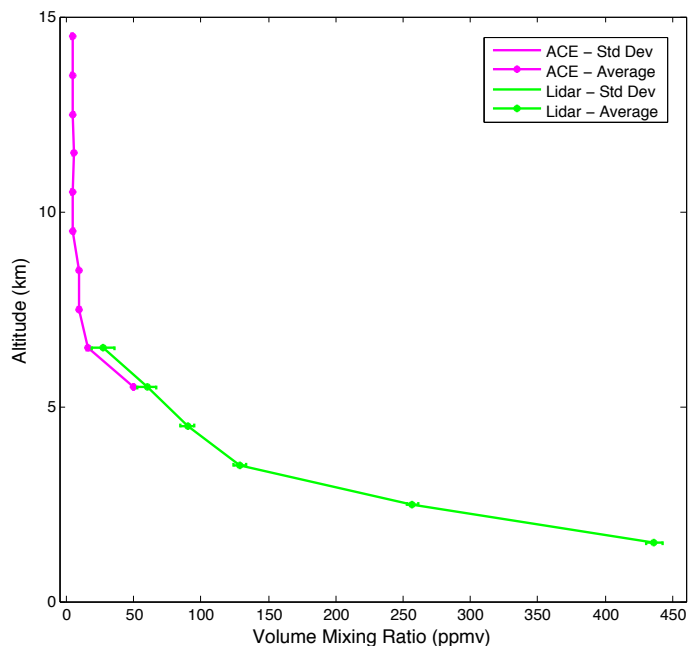


**Fig. 8.** Comparison of water vapour mixing ratio measurements made by the CEC-Lidar and ACE-FTS. The lidar profile is the average from 03:40 to 08:50 UT on the night of 28 February 2008. The ACE-FTS profile is for measurements taken at 20:40 UT near Eureka on 27 February 2008.

[Title Page](#)[Abstract](#)[Introduction](#)[Conclusions](#)[References](#)[Tables](#)[Figures](#)[◀](#)[▶](#)[◀](#)[▶](#)[Back](#)[Close](#)[Full Screen / Esc](#)[Printer-friendly Version](#)[Interactive Discussion](#)



**Calibration of the Eureka CEC water vapour lidar**

A. Moss et al.

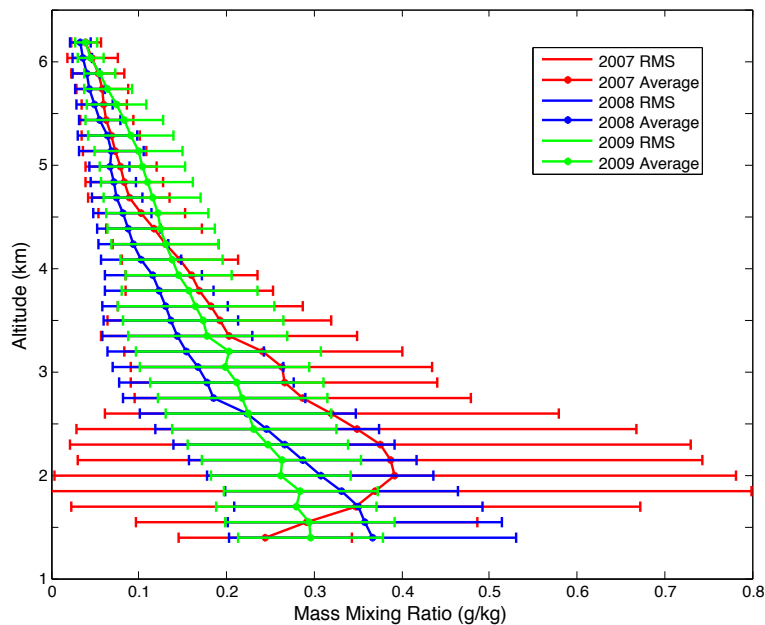


**Fig. 9.** Tropospheric water vapour mass mixing ratio climatology for the polar sunrise period (February to March) for 2007, 2008 and 2009.

Title Page

Abstract

Introduction

Conclusions

References

Tables

Figures

◀

▶

◀

▶

Back

Close

Full Screen / Esc

Printer-friendly Version

Interactive Discussion

